PCCP

Formic Acid Catalyzed Isomerization and Adduct Formation of an Isoprene-Derived Criegee Intermediate: Experiment and Theory

Journal:	*Physical Chemistry Chemical Physics*
Manuscript ID	CP-ART-09-2020-005018.R1
Article Type:	Paper
Date Submitted by the Author:	09-Nov-2020
Complete List of Authors:	Vansco, Michael; University of Pennsylvania, Chemistry Caravan, Rebecca; Argonne National Laboratory, Chemical Sciences and Engineering Pandit, Shubhrangshu; University of California San Diego, Chemistry and Biochemistry Zuraski, Kristen; NASA Jet Propulsion Laboratory, Earth Science Winiberg, Frank; NASA Jet Propulsion Laboratory, Au, Kendrew; Sandia National Laboratories, Combustion Research Facility BHAGDE, TRISHA; University of Pennsylvania School of Arts and Sciences, Chemistry Trongsiriwat, Nisalak; University of Pennsylvania, Chemistry Walsh, Patrick; UPenn, chem Osborn, David; Sandia National Laboratories, Percival, Carl; California Institute of Technology Division of Chemistry and Chemical Engineering, Jet Propulsion Laboratory Klippenstein, Stephen; Argonne National Laboratory, Chemistry Division Taatjes, Craig; Sandia National Laboratories, Lester, Marsha; University of Pennsylvania, Department of Chemistry

Formic Acid Catalyzed Isomerization and Adduct Formation of an Isoprene-Derived Criegee Intermediate: Experiment and Theory

Michael F. Vansco[1], Rebecca L. Caravan[2,3,4*], Shubhrangshu Pandit[1,5], Kristen Zuraski[2], Frank A. F. Winiberg[6,7], Kendrew Au[3], Trisha Bhagde[1], Nisalak Trongsiriwat[1], Patrick J. Walsh[1], David L. Osborn[3], Carl J. Percival[6], Stephen J. Klippenstein[4], Craig A. Taatjes[3], and Marsha I. Lester[1**]

[1]Department of Chemistry, University of Pennsylvania, Philadelphia, PA 19104-6323, USA.
[2]NASA Postdoctoral Program Fellow, NASA Jet Propulsion Laboratory, California Institute of Technology, 4800 Oak Grove Drive, Pasadena, CA 91109, USA.
[3]Combustion Research Facility, Mailstop 9055, Sandia National Laboratories, Livermore, CA 94551, USA.
[4]Chemical Sciences and Engineering Division, Argonne National Laboratory, Lemont, IL 60439, USA.
[5]Department of Chemistry and Biochemistry, University of California San Diego, La Jolla, CA 92093, USA
[6]NASA Jet Propulsion Laboratory, California Institute of Technology, 4800 Oak Grove Drive, Pasadena, CA 91109, USA.
[7]Division of Chemistry and Chemical Engineering, California Institute of Technology, Pasadena, CA 91125, USA.

Abstract

Isoprene is the most abundant non-methane hydrocarbon emitted into the Earth's atmosphere. Ozonolysis is an important atmospheric sink for isoprene, which generates reactive carbonyl oxide species ($R_1R_2C{=}O^+O^-$) known as Criegee intermediates. This study focuses on characterizing the catalyzed isomerization and adduct formation pathways for the reaction between formic acid and methyl vinyl ketone oxide (MVK-oxide), a four-carbon unsaturated Criegee intermediate generated from isoprene ozonolysis. *Syn*-MVK-oxide undergoes intramolecular 1,4 H-atom transfer to form a substituted vinyl hydroperoxide intermediate, 2-hydroperoxybuta-1,3-diene (HPBD), which subsequently decomposes to hydroxyl and vinoxylic radical products. Here, we report direct observation of HPBD generated by formic acid catalyzed isomerization of MVK-oxide under thermal conditions (298 K, 10 Torr) using multiplexed photoionization mass spectrometry. The acid catalyzed isomerization of MVK-oxide proceeds by a double hydrogen-bonded interaction followed by a concerted H-atom transfer via submerged barriers to produce HPBD and regenerate formic acid. The analogous isomerization pathway catalyzed with deuterated formic acid (D_2-formic acid) enables migration of a D atom to yield partially deuterated HPBD (DPBD), which is identified by its distinct mass (m/z 87) and photoionization threshold. In addition, bimolecular reaction of MVK-oxide with D_2-formic acid forms a functionalized hydroperoxide adduct, which is the dominant product channel, and is compared to a previous bimolecular reaction study with normal formic acid. Complementary high-level theoretical calculations are performed to further investigate the reaction pathways and kinetics.

* Corresponding author email: caravarl@anl.gov
**Corresponding author email: milester@sas.upenn.edu

I. Introduction

Criegee intermediates are reactive carbonyl oxide ($R_1R_2C=O^+O^-$) species generated from alkene ozonolysis. The reactions of Criegee intermediates formed from isoprene ozonolysis (ca. 10% of isoprene loss) are of particular interest due to the large amount of isoprene emitted into the atmosphere (ca. 600 Tg year^{-1}) from biogenic sources.[1] An important unimolecular decomposition pathway of Criegee intermediates with an alkyl group adjacent to the carbonyl oxide group is isomerization to a vinyl hydroperoxide (VHP) intermediate. This VHP is generated with sufficient internal excitation to decay to hydroxyl (OH) and vinoxy radical products.[2-6] While the products from the unimolecular decomposition of Criegee intermediates via the VHP intermediate have been detected,[2-12] validating the decomposition mechanism, studies reporting the direct detection of the VHP intermediate have been extremely limited.[13, 14] The products from the decomposition of the VHP intermediate have substantial atmospheric impact. The OH radical is the predominant tropospheric oxidant and initiates the atmospheric processing of a broad range of pollutants.[15] Vinoxy radicals primarily exist as carbon-centered radicals[16-20] that undergo rapid reaction with O_2 to form peroxy radicals.[19-23] Peroxy radicals can undergo a subsequent H-atom transfer and further reaction with O_2 to form low volatility, highly oxygenated molecules.[24-28] These autoxidation mechanisms have been implicated in the tropospheric formation of secondary organic aerosols.[29-33]

There are numerous examples in the literature in which the kinetics and branching fractions of gas-phase bimolecular reactions are shown to be influenced by the presence of additional species, for example, the water catalyzed reactions of aldehydes with OH and bimolecular reactions of Criegee intermediates.[34-41] In addition, molecular catalysis has been shown to be operative in the isomerization of Criegee intermediates to VHPs with catalysts such as water, organic acids and alcohols.[14, 42-46] In this study, we investigate the formic acid catalyzed isomerization of methyl vinyl ketone oxide ($(CH_2=CH)(CH_3)COO$, MVK-oxide), the more abundant four-carbon unsaturated Criegee intermediate produced from isoprene ozonolysis.[47] From this pathway, the substituted VHP intermediate, 2-

hydroperoxybuta-1,3-diene (HPBD), formed upon a double H-atom transfer and isomerization of MVK-oxide, is directly detected for the first time.

Calculations have revealed that MVK-oxide has four conformational forms with similar ground state energies (within ca. 3 kcal mol^{-1}), which are separated into two groups based on the orientation of the terminal oxygen with respect to the methyl group (*syn* and *anti*) and the orientation of the vinyl group with respect to the C=O group (*cis* and *trans*).[6] At 298 K the *cis* and *trans* configurations rapidly interconvert by rotation about the C-C bond, whereas interconversion between *syn* and *anti* configurations is restricted due to large barriers (ca. 30 kcal mol^{-1}).[46, 48, 49] *Syn* and *anti* conformers of MVK-oxide have very different unimolecular and bimolecular reactivity and are therefore treated as distinct chemical species.[6, 49] Previous experimental and theoretical studies have shown that *syn*-MVK-oxide undergoes slow unimolecular decay (calculated to be 33 s^{-1} at 298 K, 1 atm) via a 1,4 H-atom transfer mechanism to form HPBD, as shown in Scheme 1.[6] Unimolecular decay requires surmounting (or tunneling through) the relatively high barrier (TS1, 18.0 kcal mol^{-1}) associated with 1,4-H-atom transfer from the methyl group to the terminal O-atom of the unsaturated, four-carbon Criegee intermediate. HPBD is generated with significant internal excitation, which results in rapid homolytic cleavage of the O-O bond to form OH and 2-oxibuta-1,3-diene (OBD) radical products. OBD and OH may also follow a roaming mechanism to form 1-hydroxybut-3-en-2-one.[6]

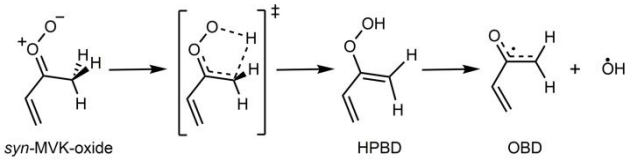

Scheme 1. Unimolecular decay mechanism of *syn*-MVK-oxide to 2-oxibuta-1,3,-diene (OBD) and OH radical products.

By contrast, *anti*-MVK-oxide is predicted to decay very rapidly (2140 s^{-1} at 298 K, 1 atm) even when thermalized. Decay occurs via an electrocyclic ring closure mechanism to generate a 5-membered cyclic peroxide known as dioxole that undergoes further unimolecular decay to oxygenated hydrocarbon radical products.[6, 48, 49] Experimental evidence of the dioxole unimolecular decay pathway has recently been

reported.[50] Although unimolecular decay via a H-atom transfer mechanism has also been considered for *anti* conformers of MVK-oxide, generating 3-hydroperoxybuta-1,2-diene (HPBD-2),[48] this involves transfer of a vinyl H-atom and has a substantially higher barrier than that for formation of dioxole. As a result, the vinyl H-atom transfer pathway is not expected to be an important unimolecular decay process for *anti*-MVK-oxide.

It is anticipated that unimolecular decay via the dioxole mechanism will be the dominant fate of *anti*-MVK-oxide in the troposphere, whereas the slower unimolecular decay of *syn*-MVK-oxide suggests that its bimolecular reactions with key atmospheric species may also be important. This has been substantiated by direct kinetic measurements of *syn*-MVK-oxide with water vapor, formic acid, and SO_2 recorded via transient absorption spectroscopy using the strong $\pi^* \leftarrow \pi$ transition of MVK-oxide.[46, 51]

In accord with theoretical predictions, reaction of *syn*-MVK-oxide with water vapor is found to be remarkably slow ($\leq 4 \times 10^{-17}$ cm^3 s^{-1} and $\leq 3 \times 10^{-14}$ cm^3 s^{-1} at 298 K, for water monomer and dimer, respectively),[46, 49, 52] such that reaction with water is not a significant tropospheric sink of *syn*-MVK-oxide. By contrast, reaction with other key atmospheric species, including formic acid and SO_2, is found to be rapid (3.0×10^{-10} cm^3 s^{-1} and 3.9×10^{-11} cm^3 s^{-1} at 298 K, respectively), comparable with observations for smaller Criegee intermediates. Global modeling reveals the reaction of *syn*-MVK-oxide with formic acid is a potentially important sink of formic acid.[46] Mass spectrometric product investigations together with high level theory demonstrate a reaction pathway leading to the formation of a functionalized hydroperoxide adduct (2-hydroperoxybut-3-en-2-yl formate, HPBF) via the 1,4-insertion of the Criegee intermediate into formic acid (Scheme 2), consistent with mechanisms observed in the reactions of smaller Criegee intermediates with organic acids.[53-60]

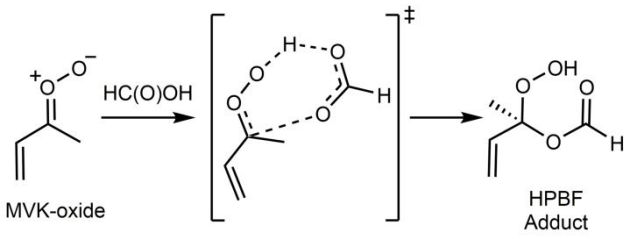

Scheme 2. Mechanism for the 1,4-insertion of MVK-oxide into formic acid.

For MVK-oxide (and other Criegee intermediates with an α-C(sp^3)–H a tom with respect to the carbonyl oxide group), an additional mechanism has been proposed for reaction with formic acid: catalyzed isomerization via a double H-atom transfer mechanism that forms a substituted VHP intermediate (Scheme 3).[42] Such functionalized hydroperoxide products have been postulated as potential precursors for the formation of secondary organic aerosols in the troposphere.[57]

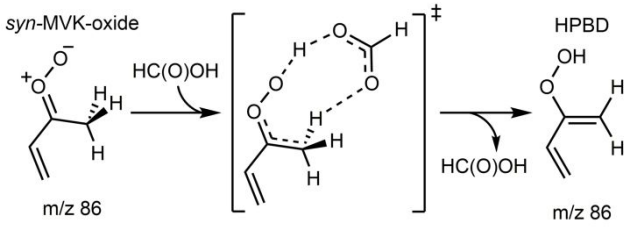

Scheme 3. Proposed mechanism for the formic acid catalyzed isomerization of *syn*-MVK-oxide to HPBD.

Prior experiments investigating the reaction of MVK-oxide with formic acid using photoionization mass spectrometry by Caravan *et al*.[46] demonstrated that the 1,4-insertion mechanism is operative. However, the acid-catalyzed mechanism producing HPBD is difficult to verify using this technique; HPBD is an isomer of MVK-oxide (and other potential products with m/z 86) and both are predicted to have similar photoionization thresholds.[6, 61] Previously, Lester and coworkers demonstrated that reaction of deuterated organic acids (RC(O)OD) with *syn*-alkyl-substituted Criegee intermediates, specifically *syn*-CH_3CHOO, $(CH_3)_2COO$, and CH_3CH_2CHOO, results in formation of partially deuterated vinyl hydroperoxide species that are distinguishable by mass from the Criegee intermediates.[14] Here, we utilize a similar approach with deuterated formic acid (D_2-formic acid) to reveal the acid-catalyzed isomerization of MVK-oxide (m/z 86) to partially deuterated HPBD (2-deuteroperoxy butadiene, DPBD) products (m/z 87). Moreover, we show that the observed threshold for photoionization of DPBD agrees with high level adiabatic ionization energy calculations,[6] thereby providing spectroscopic identification of the vinyl hydroperoxide product (HPBD) from the acid-catalyzed reaction. Finally, we provide a comprehensive theoretical examination of possible reaction pathways for *syn*- and *anti*-conformers of MVK-oxide with formic acid.

II. Experimental

Experiments are carried out using the Sandia Multiplexed Photoionization Mass Spectrometer (MPIMS) apparatus interfaced with the tunable VUV radiation of the Chemical Dynamics Beamline (9.0.2) of the Advanced Light Source (Lawrence Berkeley National Laboratory).[62] MVK-oxide is generated in the laboratory by the reaction of photolytically generated iodoalkenyl radicals with O_2 as described previously.[6, 46, 51] Specifically, vapor of the (Z/E)-1,3-diiodobut-2-ene precursor is entrained in a He flow using a pressure and temperature controlled glass bubbler (100 torr, 298 K) and mixed with O_2 (~6.4×10^{16} cm^{-3}) and deuterated formic acid (D_2-formic acid, 95% in D_2O, Fisher Scientific, 6.4×10^{12} cm^{-3}) using calibrated mass flow controllers. The gas mixture is flowed through a halocarbon wax-coated quartz reactor tube (10 torr, 298 K), and photolyzed along the length of the tube with the 248 nm output of a KrF excimer laser (100 mJ/pulse at the laser exit, ~20 mJ/pulse through the reactor). The total gas flow rate through the reactor is set such that the gas-mixture is replenished between laser pulses. The gas mixture is continuously sampled through an orifice in the reactor tube and the resultant free jet expansion is skimmed and intercepted with tunable VUV radiation. The generated ions are pulse extracted and detected using an orthogonally accelerated time-of-flight mass spectrometer. Products resulting from the MVK-oxide + D_2-formic acid reaction are investigated either by fixed ionization energy (10.5 eV) to obtain mass spectra or by scanning the photoionization energy to generate photoionization efficiency (PIE) curves (8.5-10.5 eV, 50 meV steps). Analogous experiments are conducted for the reaction of MVK-oxide with H_2-formic acid (3.2×10^{12} cm^{-3} to 1.9×10^{13} cm^{-3}, 99% Fisher Scientific) for comparison (see Supplementary Information (SI) Sec. I). The amount of H/D exchange of D_2-formic acid (m/z 48) that forms D_1-formic acid (m/z 47) is investigated under the experimental conditions by fixed ionization energy (11.5 eV) in the absence of 248 nm photolysis, and the potential impact of H/D exchange is considered in Sec. IV and SI.

III. Results

The multiple reaction pathways between MVK-oxide and formic acid were investigated using D_2-formic acid via MPIMS at 298 K and 10 torr. Both the substituted VHP product from the D_2-acid

catalyzed isomerization of MVK-oxide and HPBF adduct from the 1,4-insertion pathway are observed. As explained below, only *syn*-MVK-oxide conformers are expected to generate appreciable DPBD via the acid catalyzed pathway depicted in Scheme 4, which is distinguishable by mass from MVK-oxide. Both *syn* and *anti* conformers of MVK-oxide are expected to react rapidly with D_2-formic acid (ca. 3×10^{-10} $cm^3\ s^{-1}$)[46] via the 1,4-insertion mechanism to form a partially deuterated HPBF adduct (Scheme 5). For *anti* conformers of MVK-oxide, the bimolecular reaction with formic acid (ca. 1900 s^{-1} under the present experimental conditions) must also compete with its rapid unimolecular decay (2140 s^{-1}).

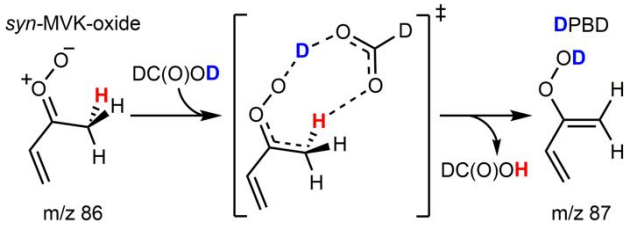

Scheme 4. D_2-formic acid catalyzed isomerization of *syn*-MVK-oxide to DPBD.

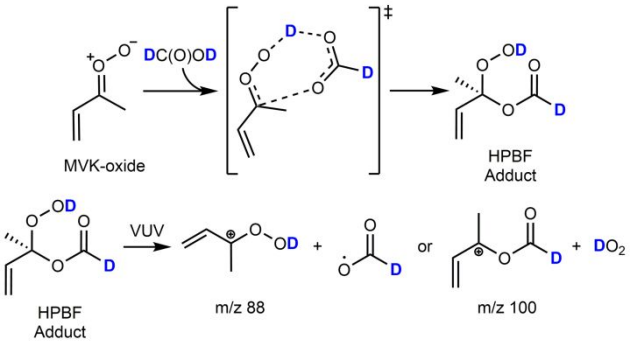

Scheme 5. Formation of the partially deuterated 1,4-insertion product from reaction between *syn*-MVK-oxide and D_2-formic acid. Photoionization with VUV radiation results in the appearance of two fragment ions (m/z 88 and 100).

Representative mass spectra obtained from the reaction of MVK-oxide with H_2-formic acid (top panel, Ref. 46) and D_2-formic acid (bottom panel) are shown in Figure 1. The 1,4-insertion product generated from the MVK-oxide + formic acid reaction undergoes fragmentation upon 10.5 eV photoionization to generate fragment ions at m/z 87 ($-HCO_2$) and m/z 99 ($-HO_2$).[46] For the MVK-oxide + D_2-formic acid reaction, deuterated analogs of the fragment ions from the 1,4-insertion product are observed (m/z 88 and 100) consistent with $-DCO_2$ and $-DO_2$ loss, respectively (Scheme 5), in accord

with Caravan *et al*.[46] Gaussian fits to the m/z 88 and 100 mass peaks yield exact masses of 88.053 ± 0.002 and 100.053 ± 0.002, respectively, confirming the chemical composition of expected fragment ions from the 1,4-insertion product ($C_4H_6O_2D$ 88.052, and $C_5H_6O_2D$ 100.052, respectively).

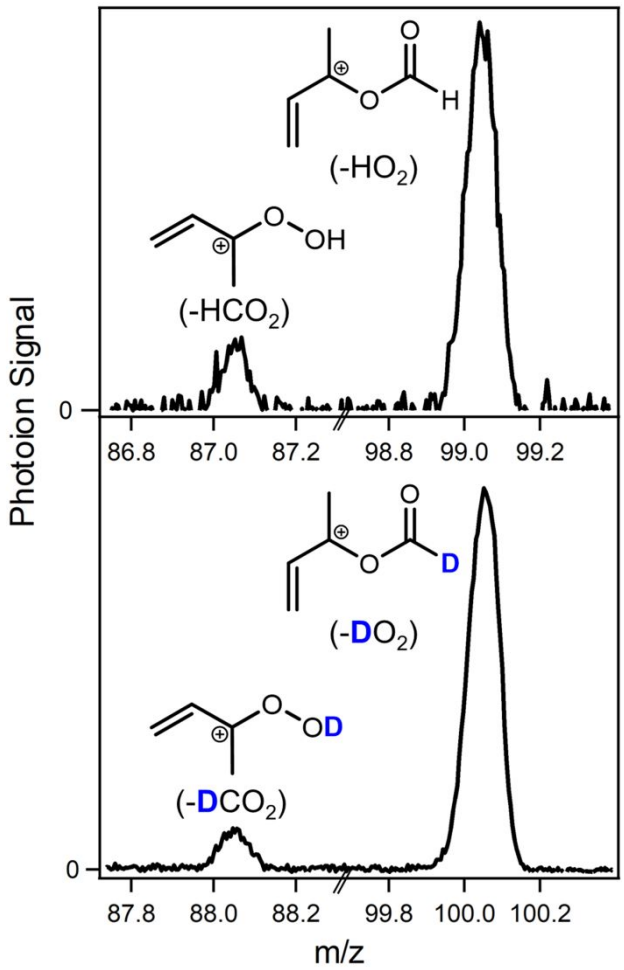

Figure 1. Comparison of fragment ions observed in mass spectra following reaction of MVK-oxide with H_2-formic acid (top panel) and D_2-formic acid (bottom panel) using MPIMS with 10.5 eV photoionization (6.4×10^{12} cm^{-3} formic acid). For H_2-formic acid (top panel), mass channels m/z 87 and 99 are attributed to $–HCO_2$ and $–HO_2$ fragment ions from the 1,4-insertion HPBF adduct, respectively. For D_2-formic acid (bottom panel), partially deuterated analogs of the fragment ions from the 1,4-insertion product are observed at m/z 88 and 100, consistent with $–DCO_2$ and $–DO_2$ loss, respectively. Data in top panel is reproduced from Caravan et al., *Proc. Natl. Acad. Sci.*, 2020, **117**, 9733-9740 (Ref. 46).

The DPBD product of the D_2-formic acid catalyzed isomerization of MVK-oxide is computed to have a much lower adiabatic ionization energy of 8.7 eV[6] compared to the computed appearance energies for the $–H/DO_2$ and $–H/DCO_2$ fragment ions (ca. 9.8 eV and 10.0 eV) from the adduct channel.[46] In order to identify the DPBD product, a mass spectrum is obtained by integration of the photoionization signal in

the 8.5-9.8 eV energy range (MPIMS, 50 meV steps) as shown in Figure 2. This energy range avoids detection of fragment ions at m/z 88 and 100 from the partially deuterated HPBF adduct (shown in Figure 1) because they are generated at higher ionization energies. The observed m/z 87 mass peak in Figure 2 is consistent with the formation of DPBD from the D_2-formic acid catalyzed isomerization of MVK-oxide (Scheme 4). A Gaussian fit to the m/z 87 mass peak yields an exact mass of 87.043 ± 0.003, in agreement with the chemical composition of DPBD ($C_4H_5O_2D$ 87.045). Additional support for the acid-catalyzed reaction mechanism from *syn*-MVK-oxide to HPBD is provided in SI (Sec. 1, Figure S1), where a growth in the photoionization signal on the m/z 86 mass channel is observed at long kinetic times with increasing H_2-formic acid concentration.

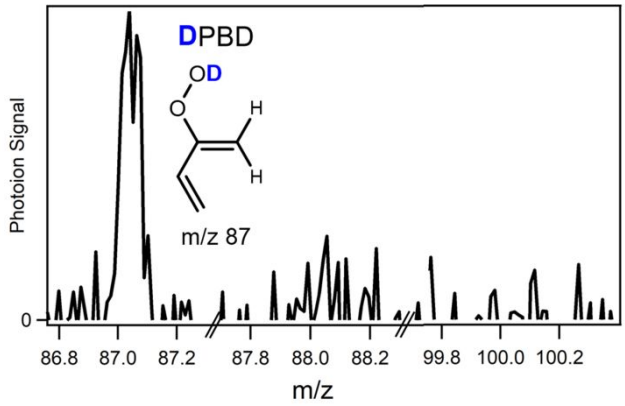

Figure 2. Mass spectrum of the DPBD (8.7 eV adiabatic ionization energy) product from the acid-catalyzed reaction of MVK-oxide with D_2-formic acid (6.4×10^{12} cm^{-3}) observed by photoionization in the 8.5-9.8 eV energy range (MPIMS, 50 meV steps). Fragment ions from the partially deuterated HPBF adduct product channel (shown in Figure 1) are not detected due to their higher appearance energies (~9.8-10 eV).[46]

Figure 3 shows the PIE curve of m/z 87 (open circles) integrated over the full kinetic time window (0-80 ms) for each VUV photon energy (8.5-10.5 eV, 50 meV steps), which reveals low and high energy components suggestive of multiple species contributing to the photoionization signal. The onset of the photoionization spectrum agrees very well with the adiabatic ionization energy computed for HPBD (8.7 eV)[6] as shown by the arrow in Figure 3. At higher energies (≥ 10.3 eV), an additional contribution to the PIE curve emerges. The origin of this signal is discussed in Sec. IV.

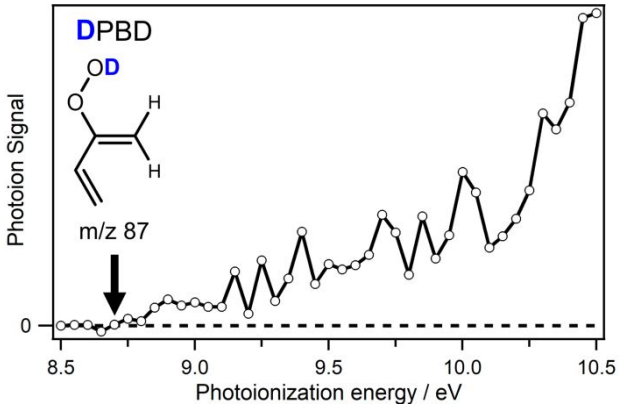

Figure 3. Photoionization efficiency curve of m/z 87 obtained by integration over the full kinetic time window (0-80 ms) using a D_2-formic acid concentration of 6.4×10^{12} cm^{-3}. The onset of photoionization signal agrees well with the adiabatic ionization energy of 8.7 eV (black arrow) computed for HPBD.[6] An additional contribution is observed at higher energies (≥ 10.3 eV) that is likely due to an isomer of HPBD.

High level *ab initio* calculations investigating the formic acid catalyzed isomerization of *syn*-MVK-oxide are carried out at the CCSD(T)-F12/CBS(TZ-F12,QZ-F12)//B2PLYP-D3/cc-pVTZ level of theory (CCSD(T)-F12/CBS). A crude estimate of the CCSDT(Q) correction for higher order excitations in the coupled cluster expansion is also incorporated. Our prior theoretical calculations to characterize the unimolecular decomposition of MVK-oxide (Scheme 1)[6] and the reaction of MVK-oxide with formic acid via the 1,4-insertion mechanism,[46] were performed at slightly different levels of theory and so those energies are redetermined here to enable a proper direct comparison of the reaction pathways (Figure 4). The formic acid catalyzed isomerization pathway has been investigated previously at the CCSD(T)/aug-cc-pVTZ//M06-2X/aug-cc-pVTZ level of theory and is compared with the present results in Sec. S2 of SI.[42]

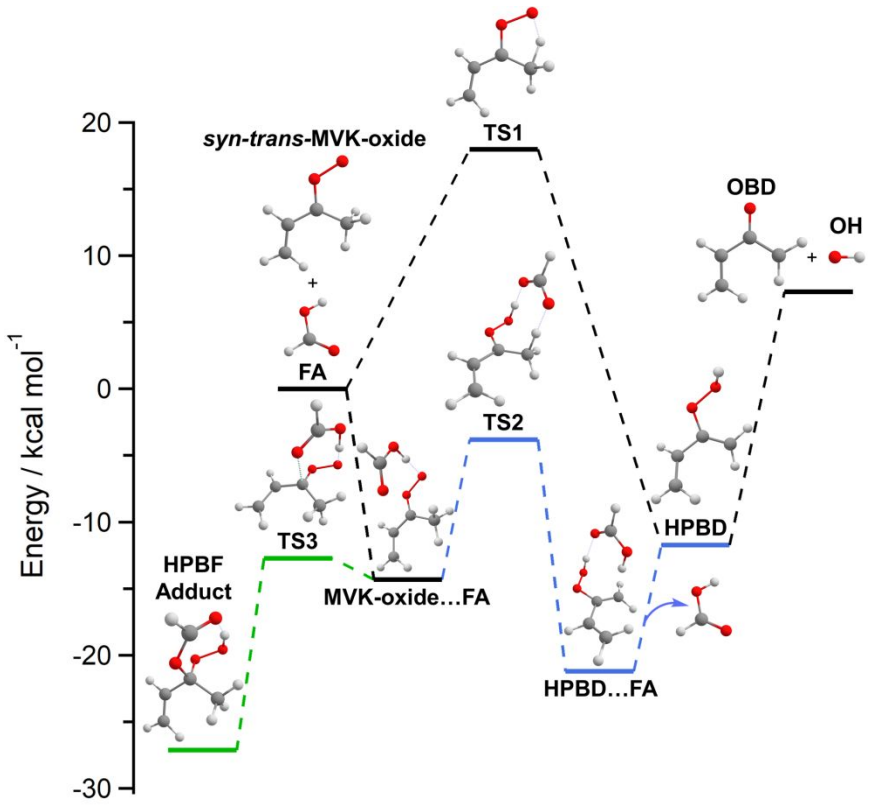

Figure 4. Reaction coordinate plot showing the unimolecular decay of *syn-trans*-MVK-oxide (black),[6] formic acid catalyzed isomerization of *syn*-MVK-oxide (blue), and HPBF adduct formation from the 1,4-insertion reaction of *syn*-MVK-oxide with formic acid (green) at the CCSD(T)-F12/CBS level of theory with an estimate of the CCSDT(Q) correction. The adduct formation pathway is reproduced from Caravan et al., *Proc. Natl. Acad. Sci.*, 2020, **117**, 9733-9740 (Ref. 46).

The current calculations indicate that both the acid catalyzed isomerization (blue) and 1,4-insertion (green) pathways begin with barrierless formation of a 7-membered cyclic pre-reactive complex (MVK-oxide…FA) that is submerged (-14.3 kcal mol^{-1}) relative to reactants. Rapid interconversion between *cis* and *trans* conformational forms of MVK-oxide within the pre-reactive complex structure is expected due to its low torsional barrier with a submerged TS ($TS_{int,cat}$, Figure S2). Acid catalyzed isomerization then proceeds via a 9-membered cyclic TS (TS2, blue) with an energy below the reactant asymptote (-4.1 kcal mol^{-1}). The intermolecular interactions at the TS facilitate a concerted movement of H atoms, in which a methyl H-atom of *syn*-MVK-oxide shifts to the carbonyl O-atom of formic acid, while the carboxylic H-atom of formic acid transfers to the terminal O-atom of MVK-oxide. A hydrogen bonded complex (HPBD…FA, -21.2 kcal mol^{-1}) is formed in the exit channel before completing the catalytic reaction with separation of the HPBD and formic acid products (-11.7 kcal mol^{-1}).

HPBF adduct formation is found to be the minimum energy reaction pathway for both *syn* (Figure 4) and *anti* (Figure S3) conformers of MVK-oxide. The TS associated with HPBF adduct formation from *syn*-MVK-oxide with formic acid is highly submerged (TS3, -12.7 kcal mol^{-1}) with a similar structure and energy as the pre-reactive complex; an analogous TS is found for *anti*-MVK-oxide. This facilitates rapid formation of the HPBF adduct and is predicted to be a significant reaction pathway for *syn* and *anti*-MVK-oxide.[46] In Sec. IV, we utilize master equation modeling to evaluate the product branching for the primary channels, acid-catalyzed reaction and adduct formation, in the MVK-oxide + formic acid reaction.

Several additional pathways for reaction of MVK-oxide with formic acid have been investigated theoretically. These pathways are illustrated in Scheme 6 with corresponding stationary point energies relative to *syn-trans*-MVK-oxide. Additional information about the electronic structure calculations, energetics, and reaction coordinates are provided in the SI (Sec. S2, Tables S1-S6 and Figures S3-S9). The additional pathways include the acid catalyzed isomerization of *anti*-MVK-oxide (Figures S3-S5), HPBF adduct formation via a 1,2-insertion mechanism (Figure S6), secondary ozonide (SOZ) formation (Figure S7), and spectator catalysis of *syn*-MVK-oxide (Figure S8).

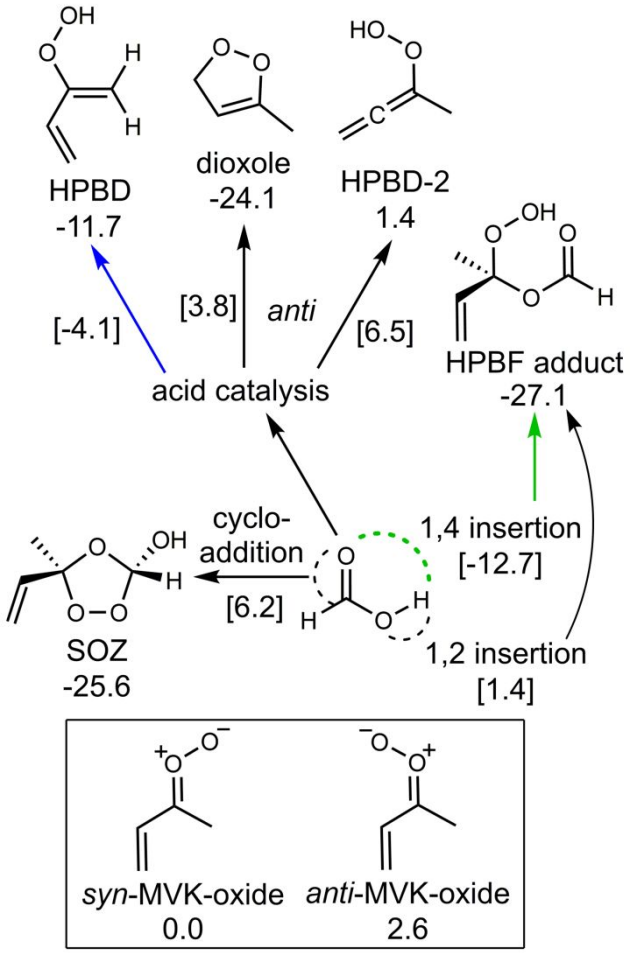

Scheme 6. Pathways for the reaction of MVK-oxide with formic acid examined theoretically with stationary point energies and transition state barriers given in kcal mol^{-1}.

The acid catalyzed isomerization of *anti*-MVK-oxide can lead to formation of dioxole, HPBD, and HPBD-2 products (Figures S3-S5). The favorable interaction between *anti*-MVK-oxide and formic acid significantly reduces the TS barrier to dioxole formation from 12.4 kcal mol^{-1} (uncatalyzed) to nearly thermoneutral (1.0 kcal mol^{-1}; acid catalyzed) relative to reactants (Figure S4). A similar low TS barrier is found for the acid catalyzed isomerization of *anti*-MVK-oxide to HPBD (-1.0 kcal mol^{-1}) relative to reactants (Figure S3). The reactive flux through these acid-catalyzed pathways is predicted to be small compared to rapid thermal unimolecular decay of *anti*-MVK-oxide to dioxole (2140 s^{-1}) and the far more favorable bimolecular reaction with acid leading to HPBF adduct formation (ca. 1900 s^{-1} under the present experimental conditions). Finally, the formic acid catalyzed isomerization of *anti*-MVK-oxide to HPBD-2 (Figure S5) is unfavorable due to a higher TS barrier for vinyl H-atom transfer (3.8 kcal mol^{-1})

relative to reactants. Additional pathways via 1,2-insertion to the HPBF adduct (Figure S6) and cycloaddition to the SOZ (Figure S7) are similarly unfavorable for MVK-oxide due to their relatively higher barriers (1.4 kcal mol^{-1} and 6.2 kcal mol^{-1}, respectively).

IV. Discussion

Two mechanisms are relevant for the reaction of *syn*-MVK-oxide with formic acid: acid catalyzed isomerization to yield a vinyl hydroperoxide (HPBD, m/z 86) and HPBF adduct formation arising from 1,4 insertion of the Criegee intermediate into formic acid. For *anti*-conformers of MVK-oxide, only HPBF adduct formation is predicted to be significant due to the higher barriers associated with its acid catalyzed isomerization process. Deuterated formic acid is utilized in this work to reveal the acid catalyzed isomerization process for *syn*-MVK-oxide. The DPBD (m/z 87) product arising from the D_2-formic acid catalyzed reaction is observed using MPIMS (above 8.7 eV); the experimental threshold energy for ionization is consistent with the theoretical adiabatic ionization energy for H/DPBD.[6] This provides experimental validation of the acid catalyzed mechanism originally proposed by Thompson and coworkers.[42] In addition, this confirms that *syn*-conformers of MVK-oxide are generated and observed under the present thermal conditions.[6, 46] The product branching for the primary channels in the *syn*-MVK-oxide + formic acid reaction, acid-catalyzed reaction and adduct formation, are examined with master equation modeling (Figures S10 and S11). Finally, this observation extends earlier studies of the acid catalyzed reaction for simple alkyl-substituted Criegee intermediates.[14]

Appearance of fragment ions on the m/z 88 ($-DCO_2$) and m/z 100 ($-DO_2$) channels is consistent with the formation of the HPBF adduct arising from the 1,4-insertion reaction of MVK-oxide with D_2-formic acid. Analogous fragment ions, m/z 87 ($-HCO_2$) and m/z 99 ($-HO_2$), are observed for the reaction with formic acid.[46] The PIE curves associated with the $-H/DO_2$ fragment ion are indistinguishable from one another (Figure S12) and both are in excellent agreement with the theoretically predicted onset for ionization (9.82 eV).[46] Thus, products from both the acid catalyzed and 1,4-insertion pathways for *syn*-MVK-oxide with formic acid are identified in the current work. Prior studies have identified the adducts

formed from the 1,4-insertion reaction of simple Criegee intermediates (CH_2OO and CH_3CHOO) with formic acid using MPIMS[55] and microwave spectroscopy.[58-60]

Previously, the (uncatalyzed) unimolecular decay of *syn*-MVK-oxide has been investigated under jet-cooled, collision-free conditions using infrared (IR) action spectroscopy.[6, 63] IR activation of *syn*-MVK-oxide with two quanta of CH stretch provides sufficient energy to surmount the transition state barrier for 1,4 H-atom transfer and generate HPBD (Scheme 1, Figure 4). The HPBD is formed with sufficient internal excitation to rapidly dissociate to OH and OBD radical products. Under thermal conditions of 298 K and 1 atm, the (uncatalyzed) unimolecular decay of *syn*-MVK-oxide follows the same reaction pathway, albeit more slowly (33 s^{-1}).[6, 46] An analogous (uncatalyzed) unimolecular decay process has been observed for d3-*syn*-MVK-oxide to OD products.[63] In contrast, the acid catalyzed isomerization of *syn*-MVK-oxide under thermal conditions will form HPBD, but it is unlikely to have sufficient energy to dissociate to OH + OBD products. The reaction follows a submerged pathway that does not require internal excitation of reactants and releases products at energies significantly below the dissociation limit. In addition, the formic acid leaving group will accept and carry away excess energy following generation of HPBD. The same would occur for reaction with D_2-formic acid, yielding DPBD, which again would be unlikely to dissociate to OD + OBD products. HPBD is similar to other functionalized hydroperoxide compounds generated from Criegee intermediate chemistry and may undergo further reactions in the atmosphere that lead to secondary organic aerosol formation,[46, 55, 57] or may eventually release OH + OBD radical products through thermal activation.[64-67]

H/D Exchange

An increase in the PIE curve at higher energies ($\geq$ 10.3 eV) is apparent in Figure 3 and suggests that more than one species contributes to the photoionization signal at m/z 87. The narrowness of the m/z 87 peak in the mass spectrum recorded at 10.5 eV (Figure S13) indicates that the interfering species has the same chemical composition as DPBD ($C_4H_5O_2D$ 87.045) and is therefore an isomer. A plausible explanation originates from reaction of MVK-oxide with partially deuterated formic acid (D_1-formic acid,

see SI). Although the D_2-formic acid from the vendor had high isotopic purity (95%), we found evidence of H/D exchange following introduction of D_2-formic acid into the flow cell (Scheme S1, Figures S13-S15, Table S7). Even with the complication arising from H/D exchange, formation of DPBD from the acid catalyzed isomerization of MVK-oxide + D_2-formic acid is clearly evident from the 8.7 eV onset of the m/z 87 PIE curve and absence of fragment ions from dissociative ionization of the HPBF adduct at photoionization energies from 8.5 to 9.8 eV.

Additional electronic structure calculations and master equation modeling were carried out to assess the possible role of H/D exchange between HPBD and D_2-formic acid under our experimental conditions. As shown in Figure S9, the barrier for isotopic exchange is significant and the associated rate constants indicate that isotopic exchange would be negligible.

Product Branching

The product branching to DPBD can be estimated by comparing the integrated photoionization signals (10.5 eV) of the acid catalyzed and adduct formation pathways. We assume the photoionization cross sections of the products are equal. In addition, it assumes that all products and fragment ions have been identified. Integration of the m/z 88 and 100 mass channels yields the photoionization signal associated with adduct formation from the MVK-oxide + D_2-formic acid reaction. Integration of the m/z 87 mass channel provides an estimate of the DPBD signal from the acid catalyzed reaction. Corrections are then made to account for contributions to the m/z 87 mass channel due to fragment ions from MVK-oxide + DC(O)OH adducts as detailed in SI.

The product branching analysis shows that HPBF adduct formation is the dominant product channel (ca. 94%), while DPBD is a minor product (ca. 6%) assuming equal populations of *syn* and *anti*-MVK-oxide under the present experimental conditions. If only *syn*-MVK-oxide is present (e.g. because of rapid unimolecular decay of *anti*-MVK-oxide), HPBF adduct formation will still be the dominant product channel (97%) compared to the acid catalyzed pathway (3%).

Thermal rate constants for the reaction of MVK-oxide with formic acid are also predicted from *ab initio* transition state theory-based master equation calculations, which are detailed in the SI. We focus on

the resultant product branching for *syn*-conformers of MVK-oxide between the acid-catalyzed pathway to HPBD with release of formic acid and the addition pathway that forms the HPBF adduct. For the experimental (T, P) conditions of 298 K and 10 torr He, the theoretical product branching ratio for the acid-catalyzed pathway is estimated to be ca. 0.3%. The product branching ratio is predicted to be strongly dependent on pressure and temperature (SI Sec. S2, Figures S10 and S11), since increased pressure and lower temperature favor stabilization of the HPBF adduct.

Notably, our calculations also indicate that the product branching ratio differs considerably for *syn-cis* and *syn-trans* conformers. Although the *syn-cis* conformer is less stable than *syn-trans* MVK-oxide (1.8 kcal mol^{-1}), their pre-reactive complexes with formic acid will rapidly equilibrate (Figure S2). As a result, the reaction of formic acid with *syn-cis* MVK-oxide will have an effectively lower submerged TS2 barrier than that for *syn-trans* MVK-oxide, resulting in enhanced acid-catalyzed reaction and reduced stabilization of the HPBF adduct (Figures S10 and S11). For *anti*-conformers of MVK-oxide, the acid-catalyzed reaction is predicted to be negligibly slow due to the higher barrier (TS2) for this pathway (Figure S3), and thus the HPBF adduct will be the dominant product channel. The barriers for other pathways (depicted in Scheme 6, Table S1) are too high for those channels to contribute significantly to the 298 K reaction.

While both experiment and theory predict that the adduct formation channel will dominate, master-equation modeling predicts a smaller contribution from the acid-catalyzed channel than experiment. Many possible uncertainties in the theoretical predictions are considered in the SI. On the experimental side, the assumption of equivalent photoionization cross sections for the products detected may be an over simplification. Deviations in photoionization cross sections among related species have been predicted theoretically,[68] but are not available for the products detected in this study.

Comparison of MVK-oxide and CH_2OO reactions with formic acid

In addition to the primary 1,4-insertion pathway for HPBF adduct formation for *syn-trans*-MVK-oxide with formic acid considered thus far, we have characterized the 1,2-insertion pathway for HPBF adduct formation and a cycloaddition pathway to secondary ozonide formation theoretically (Figures S7

and S8). The analogous reactions have been investigated for the simplest Criegee intermediate (CH_2OO) with formic acid by Vereecken at the CCSD(T)/aug-cc-pVTZ//M06-2X/aug-cc-pVTZ level of theory.[56] For *syn-trans*-MVK-oxide + formic acid, the 1,4-insertion mechanism is predicted to be substantially more favorable than 1,2-insertion because of the higher TS barrier (-12.7 and 1.4 kcal mol^{-1}, respectively), as found previously for the reaction of CH_2OO with formic acid. However, the HPBF adduct formed from the *syn*-MVK-oxide + formic acid reaction is much less stable than its CH_2OO analog (-27.4 kcal mol^{-1} vs -44.4 kcal mol^{-1}, respectively, Tables S3 and S4) due to disruption of the resonance stabilization present in MVK-oxide.[46]

SOZ generation from the cycloaddition reaction of *syn*-MVK-oxide with formic acid further demonstrates the impact of resonance stabilization of MVK-oxide on its reactivity. The pre-reactive complex formed between *syn-trans*-MVK-oxide and formic acid is more strongly bound than its CH_2OO analog (-14.3 vs -6.0 kcal mol^{-1}, respectively, Table S5), likely due to stronger dispersion forces in the MVK-oxide pre-reactive complex. However, disruption of the resonance stability of MVK-oxide at the transition state results in a much higher barrier for SOZ formation than found for CH_2OO (6.2 vs -1.7 kcal mol^{-1}, respectively). Moreover, the SOZ formed from the reaction of *syn-trans*-MVK-oxide with formic acid is much less stable than its CH_2OO analog (-26.7 vs. -40.2 kcal mol^{-1}, respectively, Table S5). Overall, HPBF adduct formation from the 1,4-insertion mechanism is the primary reaction pathway for both *syn*- and *anti*-conformers of MVK-oxide with formic acid; formic acid catalyzed isomerization provides an alternate but less favorable pathway for *syn*-MVK-oxide.

Conclusion

High level *ab initio* calculations predict two active mechanisms for reaction of MVK-oxide with formic acid: (1) bimolecular reaction of formic acid with both *syn*- and *anti*-conformers of MVK-oxide via a 1,4-insertion mechanism that generates a functionalized hydroperoxide[46] and (2) formic acid catalyzed isomerization of *syn*-MVK-oxide via a barrierless double H-atom transfer mechanism to form vinyl hydroperoxide (HPBD) with regeneration of formic acid.[42] In this study, we demonstrate that reaction of deuterated formic acid with MVK-oxide in a flow cell (298 K, 10 Torr) with photoionization

(MPIMS) detection enables identification of both the adduct formation and acid catalyzed reaction pathways. Previously, the HPBF adduct was shown to be a primary product of the reaction of MVK-oxide with formic acid.[46] Specifically, dissociative photoionization of the HPBF adduct was observed by identification of fragment ions associated with $-HCO_2$ and $-HO_2$ loss processes. Here, the partially deuterated HPBF adduct from reaction of MVK-oxide with D_2-formic acid is observed through analogous fragment ions ($-DCO_2$ at m/z 88 and $-DO_2$ at m/z 100) associated with dissociative photoionization. The PIE curves for the fragment ions from reaction with D_2-formic acid agree with those reported previously for reaction with formic acid,[46] providing further support for the formation of the partially deuterated HPBF adduct in the MVK-oxide + D_2-formic acid reaction.

In addition, the formic acid catalyzed isomerization pathway is revealed using D_2-formic acid, which is identified for the first time. D-atom transfer from the acid to *syn*-MVK-oxide yields a partially deuterated vinyl hydroperoxide (DPBD), which is identified through MPIMS by its distinct mass (m/z 87) and photoionization threshold. The analogous pathway with H_2-formic acid would appear at the same m/z as MVK-oxide, which makes it difficult to observe. The onset energy at ca. 8.7 eV observed for photoionization of the DPBD products (m/z 87) from the acid catalyzed isomerization of *syn*-MVK-oxide is in good accord with a prior high level theoretical calculation of the adiabatic ionization energy of HPBD (8.7 eV).[6] The product branching is estimated from the magnitude of the ionization signals (assuming similar photoionization cross sections). This indicates that the HPBF adduct is the dominant product channel (94%) and the acid catalyzed isomerization to DPBD is a minor channel (6%), assuming equal populations of *syn* and *anti*-MVK-oxide are generated under the present experimental conditions and equal photoionization cross sections. High-level *ab initio* calculations indicate HPBF adduct formation is strongly favored compared to acid catalyzed isomerization, consistent with the experimental results.

Acknowledgements

This research was supported by the U.S. Department of Energy-Basic Energy Sciences under grant DE-FG02-87ER13792 (MIL). This material is also based upon work supported by the Division of Chemical Sciences, Geosciences and Biosciences, Office of Basic Energy Sciences (BES), U.S. Department of Energy (USDOE). Sandia National Laboratories is a multimission laboratory managed and operated by National Technology and Engineering Solutions of Sandia, LLC., a wholly owned subsidiary of Honeywell International, Inc., for the USDOE's National Nuclear Security Administration under contract DE-NA0003525. This paper describes objective technical results and analysis. Any subjective views or opinions that might be expressed in the paper do not necessarily represent the views of the USDOE or the United States Government. This material is based in part on research at Argonne supported by the U.S. Department of Energy, Office of Science, Office of Basic Energy Sciences, Division of Chemical Sciences, Geosciences, and Biosciences under Contract No. DE-AC02-06CH11357. The Advanced Light Source is supported by the Director, Office of Science, BES/USDOE under Contract DE- AC02-05CH11231 at Lawrence Berkeley National Laboratory. This research was carried out in part by the Jet Propulsion Laboratory, California Institute of Technology, under contract with the National Aeronautics and Space Administration (NASA), supported by the Upper Atmosphere Research and Tropospheric Chemistry program. The contributions of RLC and KZ were in part supported by appointments to the NASA Postdoctoral Program at the NASA Jet Propulsion Laboratory, administered by Universities Space Research Association under contract with NASA. PJW thanks the NSF (CHE-1902509).

We are grateful to Dr. Leonid Sheps (Sandia) and Dr. Ahren Jasper (Argonne) for useful discussions.

References

1. K. Sindelarova, C. Granier, I. Bouarar, A. Guenther, S. Tilmes, T. Stavrakou, J. F. Müller, U. Kuhn, P. Stefani and W. Knorr, *Atmos. Chem. Phys.*, 2014, **14**, 9317-9341.
2. F. Liu, J. M. Beames, A. S. Petit, A. B. McCoy and M. I. Lester, *Science*, 2014, **345**, 1596-1598.
3. F. Liu, J. M. Beames and M. I. Lester, *J. Chem. Phys.*, 2014, **141**, 234312.
4. Y. Fang, F. Liu, S. J. Klippenstein and M. I. Lester, *J. Chem. Phys.*, 2016, **145**, 044312.
5. Y. Fang, F. Liu, V. P. Barber, S. J. Klippenstein, A. B. McCoy and M. I. Lester, *J. Chem. Phys.*, 2016, **144**, 061102.
6. V. P. Barber, S. Pandit, A. M. Green, N. Trongsiriwat, P. J. Walsh, S. J. Klippenstein and M. I. Lester, *J. Am. Chem. Soc.*, 2018, **140**, 10866-10880.
7. Y. Fang, F. Liu, V. P. Barber, S. J. Klippenstein, A. B. McCoy and M. I. Lester, *J. Chem. Phys.*, 2016, **145**, 234308.
8. Y. Fang, V. P. Barber, S. J. Klippenstein, A. B. McCoy and M. I. Lester, *J. Chem. Phys.*, 2017, **146**, 134307.
9. V. P. Barber, S. Pandit, V. J. Esposito, A. B. McCoy and M. I. Lester, *J. Phys. Chem. A*, 2019, **123**, 2559-2569.
10. V. P. Barber, V. J. Esposito, T. Trabelsi, A. S. Hansen, T. A. McHenry, J. S. Francisco and M. I. Lester, *Chem. Phys. Lett.*, 2020, **751**, 137478.
11. M. I. Lester and S. J. Klippenstein, *Acc. Chem. Res.*, 2018, **51**, 978-985.
12. T. A. Stephenson and M. I. Lester, *Int. Rev. Phys. Chem.*, 2020, **39**, 1-33.
13. A. Bagchi, Y. Yu, J.-H. Huang, C.-C. Tsai, W.-P. Hu and C. C. Wang, *Phys. Chem. Chem. Phys.*, 2020, **22**, 6528-6537.
14. F. Liu, Y. Fang, M. Kumar, W. H. Thompson and M. I. Lester, *Phys. Chem. Chem. Phys.*, 2015, **17**, 20490-20494.
15. B. J. Finlayson-Pitts and J. N. Pitts, *Chemistry of the Upper and Lower Atmosphere*, Academic Press, San Diego, 2000.
16. G. Inoue and H. Akimoto, *J. Chem. Phys.*, 1981, **74**, 425-433.
17. M. Dupuis, J. J. Wendoloski and W. A. Lester Jr., *J. Chem. Phys.*, 1982, **76**, 488-492.
18. M. E. Jacox, *Chem. Phys.*, 1982, **69**, 407-422.
19. J. D. Weidman, R. T. Allen, K. B. MooreIII and H. F. Schaefer III, *J. Chem. Phys.*, 2018, **148**, 184308.
20. M. M. Davis, J. D. Weidman, A. S. Abbott, G. E. Douberly, J. M. Turney and H. F. Schaefer III, *J. Chem. Phys.*, 2019, **151**, 124302.
21. T. Oguchi, A. Miyoshi, M. Koshi, H. Matsui and N. Washida, *J. Phys. Chem. A*, 2001, **105**, 378-382.
22. M. Hassouna, E. Delbos, P. Devolder, B. Viskolcz and C. Fittschen, *J. Phys. Chem. A*, 2006, **110**, 6667-6672.
23. E. Delbos, C. Fittschen, H. Hippler, N. Krasteva, M. Olzmann and B. Viskolcz, *J. Phys. Chem. A*, 2006, **110**, 3238-3245.
24. J. J. Orlando and G. S. Tyndall, *Chem. Soc. Rev.*, 2012, **41**, 6294-6317.
25. K. H. Møller, K. H. Bates and H. G. Kjaergaard, *J. Phys. Chem A*, 2019, **123**, 920-932.
26. E. Praske, R. V. Otkjaer, J. D. Crounse, J. C. Hethcox, B. M. Stoltz, H. G. Kjaergaard and P. O. Wennberg, *J. Phys. Chem. A*, 2019, **123**, 590-600.
27. R. V. Otkjaer, H. H. Jakobsen, C. M. Tram and H. G. Kjaergaard, *J. Phys. Chem. A*, 2018, **122**, 8665-8673.
28. K. H. Møller, T. Berndt and H. G. Kjaergaard, *Environ. Sci. Technol.*, 2020, **54**, 11087-11099.
29. F. Paulot, J. D. Crounse, H. G. Kjaergaard, A. Kürten, J. M. St Clair, J. H. Seinfeld and P. O. Wennberg, *Science*, 2009, **325**, 730-733.
30. J. D. Crounse, L. B. Nielsen, S. Jørgensen, H. G. Kjaergaard and P. O. Wennberg, *J. Phys. Chem. Lett.*, 2013, **4**, 3513-3520.

31. M. Ehn, J. A. Thornton, E. Kleist, M. Sipilä, H. Junninen, I. Pullinen, M. Springer, F. Rubach, R. Tillmann, B. Lee, F. Lopez-Hilfiker, S. Andres, I.-H. Acir, M. Rissanen, T. Jokinen, S. Schobesberger, J. Kangasluoma, J. Kontkanen, T. Nieminen, T. Kurtén, L. B. Nielsen, S. Jørgensen, H. G. Kjaergaard, M. Canagaratna, M. D. Maso, T. Berndt, T. Petäjä, A. Wahner, V.-M. Kerminen, M. Kulmala, D. R. Worsnop, J. Wildt and T. F. Mentel, *Nature*, 2014, **506**, 476.
32. T. Jokinen, M. Sipilä, S. Richters, V.-M. Kerminen, P. Paasonen, F. Stratmann, D. R. Worsnop, M. Kulmala, M. Ehn, H. Herrmann and T. Berndt, *Angew. Chem. Int. Ed.*, 2014, **53**, 14596-14600.
33. K. C. Barsanti, J. H. Kroll and J. A. Thornton, *J. Phys. Chem. Lett.*, 2017, **8**, 1503-1511.
34. E. Vöhringer-Martinez, B. Hansmann, H. Hernandez, J. S. Francisco, J. Troe and B. Abel, *Science*, 2007, **315**, 497-501.
35. W. Zhang, B. Du and Z. Qin, *J. Phys. Chem A*, 2014, **118**, 4797-4807.
36. T. R. Lewis, M. A. Blitz, D. E. Heard and P. W. Seakins, *Phys. Chem. Chem. Phys.*, 2015, **17**, 4859-4863.
37. L. Sheps, B. Rotavera, A. J. Eskola, D. L. Osborn, C. A. Taatjes, K. Au, D. E. Shallcross, M. A. H. Khan and C. J. Percival, *Phys. Chem. Chem. Phys.*, 2017, **19**, 21970-21979.
38. T. A. Burd, X. Shan and D. C. Clary, *Phys. Chem. Chem. Phys.*, 2018, **20**, 25224-25234.
39. M. Kumar, A. Sinha and J. S. Francisco, *Acc. Chem. Res.*, 2016, **49**, 877-883.
40. W. Chao, C. Yin, K. Takahashi and J. J. M. Lin, *Phys. Chem. Chem. Phys.*, 2019, **21**, 22589-22597.
41. W. Chao, C. T. Yin, K. Takahashi and J. J. M. Lin, *J. Phys. Chem A*, 2019, **123**, 8336-8348.
42. M. Kumar, D. H. Busch, B. Subramaniam and W. H. Thompson, *Phys. Chem. Chem. Phys.*, 2014, **16**, 22968-22973.
43. B. Long, J. L. Bao and D. G. Truhlar, *J. Am. Chem. Soc.*, 2016, **138**, 14409-14422.
44. M. Monge-Palacios, M. P. Rissanen, Z. Wang and S. M. Sarathy, *Phys. Chem. Chem. Phys.*, 2018, **20**, 10806-10814.
45. N. A. I. Watson, J. A. Black, T. M. Stonelake, P. J. Knowles and J. M. Beames, *J. Phys. Chem. A*, 2019, **123**, 218-229.
46. R. L. Caravan, M. F. Vansco, K. Au, M. A. H. Khan, Y.-L. Li, F. A. F. Winiberg, K. Zuraski, Y.-H. Lin, W. Chao, N. Trongsiriwat, P. J. Walsh, D. L. Osborn, C. J. Percival, J. J.-M. Lin, D. E. Shallcross, L. Sheps, S. J. Klippenstein, C. A. Taatjes and M. I. Lester, *Proc. Natl. Acad. Sci.*, 2020, **117**, 9733-9740.
47. T. B. Nguyen, G. S. Tyndall, J. D. Crounse, A. P. Teng, K. H. Bates, R. H. Schwantes, M. M. Coggon, L. Zhang, P. Feiner, D. O. Milller, K. M. Skog, J. C. Rivera-Rios, M. Dorris, K. F. Olson, A. Koss, R. J. Wild, S. S. Brown, A. H. Goldstein, J. A. de Gouw, W. H. Brune, F. N. Keutsch, J. H. Seinfeld and P. O. Wennberg, *Phys. Chem. Chem. Phys.*, 2016, **18**, 10241-10254.
48. K. T. Kuwata, L. C. Valin and A. D. Converse, *J. Phys. Chem. A*, 2005, **109**, 10725.
49. L. Vereecken, A. Novelli and D. Taraborrelli, *Phys. Chem. Chem. Phys.*, 2017, **19**, 31599-31612.
50. M. F. Vansco, R. L. Caravan, K. Zuraski, F. A. F. Winiberg, K. Au, N. Trongsiriwat, P. J. Walsh, D. L. Osborn, C. J. Percival, M. A. H. Khan, D. E. Shallcross, C. A. Taatjes and M. I. Lester, *J. Phys. Chem A*, 2020, **124**, 3542-3554.
51. M. F. Vansco, B. Marchetti and M. I. Lester, *J. Chem. Phys.*, 2018, **149**, 244309.
52. J. M. Anglada and A. Solé, *Phys. Chem. Chem. Phys.*, 2016, **18**, 17698-17712.
53. P. Aplincourt and M. F. Ruiz-López, *J. Phys. Chem. A*, 2000, **104**, 380-388.
54. B. Long, J.-R. Cheng, X.-f. Tan and W.-j. Zhang, *J. Mol. Struc-THEOCHEM*, 2009, **916**, 159-167.
55. O. Welz, A. J. Eskola, L. Sheps, B. Rotavera, J. D. Savee, A. M. Scheer, D. L. Osborn, D. Lowe, A. Murray Booth, P. Xiao, M. Anwar H. Khan, C. J. Percival, D. E. Shallcross and C. A. Taatjes, *Angew. Chem. Int. Ed.*, 2014, **53**, 4547-4550.
56. L. Vereecken, *Phys. Chem. Chem. Phys.*, 2017, **19**, 28630-28640.

57. R. Chhantyal-Pun, B. Rotavera, M. R. McGillen, M. A. H. Khan, A. J. Eskola, R. L. Caravan, L. Blacker, D. P. Tew, D. L. Osborn, C. J. Percival, C. A. Taatjes, D. E. Shallcross and A. J. Orr-Ewing, *ACS Earth and Space Chem.*, 2018, **2**, 833-842.
58. J. P. Porterfield, K. L. K. Lee, V. Dell'Isola, P. B. Carroll and M. C. McCarthy, *Phys. Chem. Chem. Phys.*, 2019, **21**, 18065-18070.
59. C. Cabezas and Y. Endo, *Phys. Chem. Chem. Phys.*, 2019, **21**, 18029-18408.
60. C. Cabezas and Y. Endo, *Phys. Chem. Chem. Phys.*, 2020, **22**, 446-454.
61. C. A. Taatjes, F. Liu, B. Rotavera, M. Kumar, R. Caravan, D. L. Osborn, W. H. Thompson and M. I. Lester, *J. Phys. Chem. A*, 2017, **121**, 16-23.
62. D. L. Osborn, P. Zou, H. Johnsen, C. C. Hayden, C. A. Taatjes, V. D. Knyazev, S. W. North, D. S. Peterka, M. Ahmed and S. R. Leone, *Rev. Sci. Instrum.*, 2008, **79**, 104103.
63. A. S. Hansen, Z. Liu, S. Chen, M. G. Schumer, P. J. Walsh and M. I. Lester, *J. Phys. Chem A*, 2020, **124**, 4929-4938.
64. N. M. Donahue, G. T. Drozd, S. A. Epstein, A. A. Presto and J. H. Kroll, *Phys. Chem. Chem. Phys.*, 2011, **13**, 10848-10857.
65. G. T. Drozd, J. Kroll and N. M. Donahue, *J. Phys. Chem. A*, 2011, **115**, 161-166.
66. T. Kurten and N. M. Donahue, *J. Phys. Chem. A*, 2012, **116**, 6823-6830.
67. K. T. Kuwata, L. Luu, A. B. Weberg, K. Huang, A. J. Parsons, L. A. Peebles, N. B. Rackstraw and M. J. Kim, *J. Phys. Chem. A*, 2018, **122**, 2485-2502.
68. C. Huang, B. Yang and F. Zhang, *J. Chem. Phys.*, 2019, **150**, 164305.

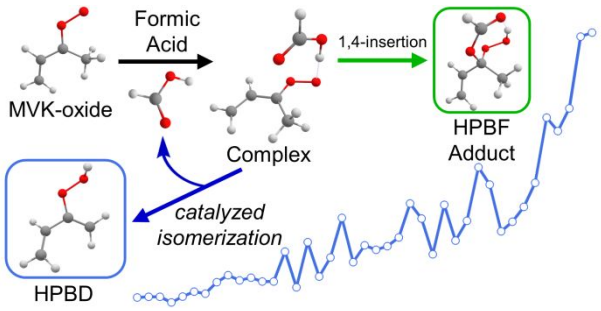

Investigation of key reaction pathways for an isoprene-derived Criegee intermediate with formic acid: acid catalyzed isomerization and adduct formation.